CHINESE OPTICS LETTERS

Vol. 21, No. 9 | September 2023

Four-channel metasurface for multiplexing images under two nonorthogonal polarization states

Wenyuan Liu (刘文远), Yizhou Zhuo (卓奕州), Likun Xiao (肖莉琨), Chen Chen (陈 晨), Shu Shang (尚 书), Hongzhan Liu (刘宏展), Hongyun Meng (蒙红云), Faqiang Wang (王发强), Xiangbo Yang (杨湘波), and Zhongchao Wei (韦中超)*

Guangdong Provincial Key Laboratory of Nanophotonic Functional Materials and Devices, School of Information and Optoelectronic Science and Engineering, South China Normal University, Guangzhou 510006, China

*Corresponding author: wzc@scnu.edu.cn

Received May 26, 2023 | Accepted June 15, 2023 | Posted Online August 21, 2023

By its unparalleled capacity to manipulate optical parameters, metasurfaces demonstrate the ability to simultaneously manipulate the amplitude and phase of incident light. Exhibiting both near-field nanoprinting images and far-field holography images is a quintessential illustration of this capability. In preceding investigations, image multiplexing commonly transpires within the single polarization state or orthogonal polarization states, thereby exhibiting a deficiency in terms of information security when contrasted with the nonorthogonal polarization states. In this research, a multifunctional metasurface with the capability of exhibiting four-channel images has been proposed by using a nanobrick as a quarter-wave plate. Through the adjustment of the orientation angles of each nanobrick, nanoprinting can be displayed under both linearly and circularly polarized light. Building on this, the propagation phase is combined with the geometric phase to generate diverse phase delays, enabling the metasurface to be multiplexed under two nonorthogonal polarization states to achieve four-channel image displays. Intriguingly, bidirectional nanoprinting and bidirectional holography can be achieved by altering the direction of incidence polarization states. The proposed metasurface platform can open new possibilities for creating compact multifunctional optical devices, while also enhancing applications in multichannel image displays, information anticounterfeiting, and encryption.

Keywords: holography; nanoprinting; quarter-wave plate; multiplexing.
DOI: 10.3788/COL202321.093601

1. Introduction

Metasurfaces are artificially designed planar structures that have demonstrated the remarkable ability to effectively manipulate the amplitude[1–3], phase[4–9], and polarization[10–15] of incident optical waves. With the continuous evolution of integrated optics, metasurfaces that possess the ability to simultaneously modulate multiple properties of incident light have been proposed as candidates for data storage and information encryption[16]. Exhibiting both near-field nanoprinting images and far-field holography images[17–25] is a quintessential illustration of manipulating the amplitude and phase concurrently. In order to achieve these operations, prior investigations have employed three major approaches. The first entails adjusting the transmittance to generate a nanoprinting image and altering the orientation angles of the nanobricks to produce a holographic image[26]. The second approach employs Malus's law and propagation phase to display two images in two fields at the same time[27,28]. The final approach involves utilizing structural color to exhibit both a color nanoprinting image and a full-color holographic image simultaneously[29].

Information multiplexing can make the maximal use of existing metasurfaces[30–32] to improve the information capacity as much as possible without increased costs. Previous studies have demonstrated the feasibility of displaying images in two fields under a single incident polarization state. Additionally, recent research has demonstrated that interleaved metasurfaces[33] and coherent pixelated metasurfaces[34] can be multiplexed under two polarization states to achieve four-channel image displays. Polarization multiplexing is generally conducted in two orthogonal polarization states. This can be attributed to the inherent inability of two orthogonal polarization beams to interfere with one another. The process of multiplying images under two nonorthogonal polarization states has emerged as a pressing necessity in multichannel image displays, which offers heightened information security compared to those based on orthogonal polarization states. In recent years, the presentation

of dual-channel nanoprinting under two nonorthogonal states has been displayed by leveraging the orientation degeneracy[35,36] implicit in Malus's law. Nevertheless, this approach merely involves manipulating amplitude and does not enable image multiplexing. Multiplying images under two nonorthogonal polarization states has become an urgent need in multichannel image displays.

This work proposes a single-layer metasurface platform to achieve the effect of four-channel image displays under two nonorthogonal polarization states. In contrast to previous demonstrations, the anisotropic nanobricks act as quarter-wave plates (QWPs)[37]. By tailoring the orientation angles of each nanobrick, nanoprinting can be displayed under both linearly polarized (LP) light and circularly polarized (CP) light. This provides a novel method to achieve dual-channel image displays and enhance the design's flexibility. Building on this, the propagation phase is combined with the geometric phase to generate different phase delays, enabling the metasurface to be multiplexed under two nonorthogonal polarization states to achieve four-channel image displays. A single-layer metasurface composed of subwavelength-spaced silicon (Si) nanobricks on a silicon dioxide (SiO_2) substrate is designed to demonstrate this capability. Each nanobrick of this single-layer metasurface integrates two sets of amplitude- and phase-modulated channels. Moreover, bidirectional nanoprinting and bidirectional holography can be achieved by changing the direction of incidence polarization states. This provides a simple way to implement bidirectional nanoprinting and bidirectional holography, enhancing their practical applications. The proposed metasurface platform can open new possibilities of creating compact multifunctional optical devices, while also enhancing applications in multichannel image displays, information anticounterfeiting, and encryption.

2. Design Principle

As shown in Fig. 1, the metasurface displays the ability to manipulate the amplitude and phase of two nonorthogonal polarization states. Upon incidence of LP light, "petal" and "C" patterns are discernible, while CP light incidence reveals "A" and "B" patterns.

In the near field, we contemplate the methodology of displaying a nanoprinting image under LP light first and then displaying a nanoprinting image under CP light. The required Jones matrix is calculated as

$$J = R(-\theta)\begin{bmatrix} t_x e^{i\phi_x} & 0 \\ 0 & t_y e^{i\phi_y} \end{bmatrix} R(\theta), \tag{1}$$

where $R(\theta)$ indicates the rotation matrix. θ is the in-plane orientation angle of the nanobrick. t_x and t_y are the transmission coefficients. ϕ_x and ϕ_y are the polarization-dependent phase shifts. When the polarization direction of the polarizer is fixed at $\pi/2$, the polarization state of the incident light is y-polarized (YLP) light. Upon incidence onto the metasurface, the complex-amplitude of the output light can be expressed as

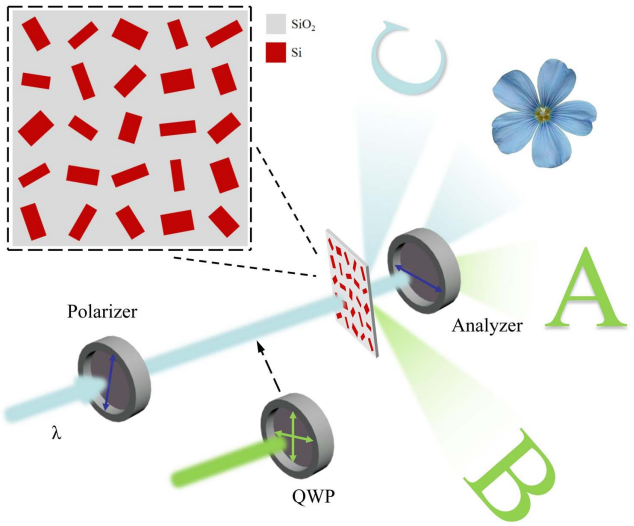

Fig. 1. Operation schematic of four-channel metasurface. The metasurface is composed of Si nanobricks with five different structures and different orientation angles. The four images are showcased on two separate channels. Channel 1 exhibits a continuous-brightness nanoprinting image and a holography image, both of which are acquired via LP light. Channel 2 displays a binary-brightness nanoprinting image and a holography image acquired via CP light. The polarizer is used to derive LP light for channel 1, whereas a combination of a polarizer and a QWP is utilized to extract CP light for channel 2.

$$E_1 = [(t_x e^{i\phi_x} - t_y e^{i\phi_y}) \sin\theta \cos\theta, t_x e^{i\phi_x} \sin^2\theta + t_y e^{i\phi_y} \cos^2\theta]^T. \tag{2}$$

When the output light goes through an analyzer with a fixed polarization direction of 0° again, the intensity of output light can be expressed as

$$I_1 = \left| \frac{t_x e^{i\phi_x} - t_y e^{i\phi_y}}{2} \right|^2 \sin^2(2\theta). \tag{3}$$

Subsequently, a QWP is positioned behind the polarizer, whereby it influences the transformation of the incident light from a YLP light to a left circularly polarized (LCP) light. Upon incidence onto the metasurface, the complex-amplitude of the output light can be expressed as

$$E_2 = \frac{1}{\sqrt{2}}\left(\frac{t_x e^{i\phi_x} + t_y e^{i\phi_y}}{2}[1,i]^T + \frac{t_x e^{i\phi_x} - t_y e^{i\phi_y}}{2} e^{2i\theta}[1,-i]^T \right). \tag{4}$$

Likewise, as the output light is transmitted through the analyzer once more, the intensity of output light can be expressed as

$$I_2 = \frac{1}{2}\left| \frac{t_x e^{i\phi_x} + t_y e^{i\phi_y}}{2} + \frac{t_x e^{i\phi_x} - t_y e^{i\phi_y}}{2} e^{2i\theta} \right|^2. \tag{5}$$

It is obvious that the magnitude of the output light is contingent upon the orientation angle of the nanobrick when

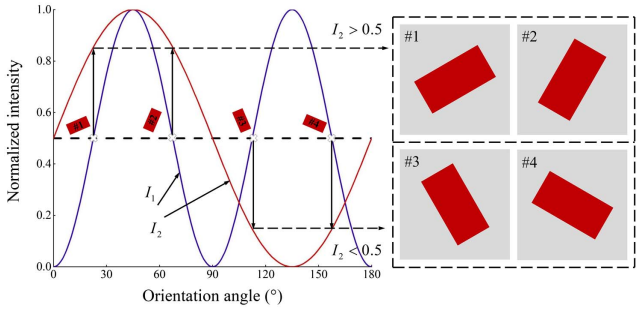

Fig. 2. Working principle of displaying dual-channel nanoprinting images. The intensity of the output light can be modulated by two different modulation functions, namely, I_1 and I_2. To attain a specific intensity modulation for nanoprinting target 1, four orientation options are available for each nanobrick. The selection of the appropriate orientation is based on whether the intensity of nanoprinting target 2 is lower or higher than 0.5, whereby only two out of four orientations are deemed eligible.

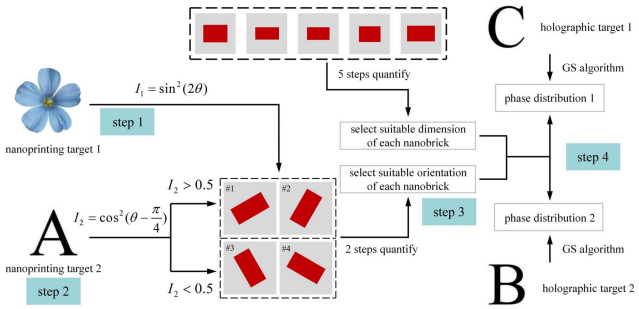

Fig. 3. The design process for a four-channel metasurface. First, in order to achieve a specific intensity modulation of the nanoprinting target 1, one may choose from four different orientation angles. Second, by selecting two orientation angles based on whether the intensity of nanoprinting target 2 is lower or higher than 0.5, two-step geometric phase encoding can be attained. Subsequently, the propagation phase can be combined with the geometric phase to generate different phase delays for both YLP and LCP incident light. Finally, the GS algorithm can be employed to calculate the target phase. From the 10-step phases mentioned above, select the one closest to the two holographic images.

$|t_x e^{i\phi_x} + t_y e^{i\phi_y}|$ is not equal to zero. The maximum intensity interval of the output light can be covered when $|t_x e^{i\phi_x} + t_y e^{i\phi_y}| = |t_x e^{i\phi_x} - t_y e^{i\phi_y}|$. In such a scenario, the anisotropic nanobricks act as QWPs, and the intensity of the output light can be simplified as

$$I_1 = \frac{1}{2}\sin^2(2\theta), \quad I_2 = \cos^2\left(\theta - \frac{\pi}{4}\right). \tag{6}$$

The operational mechanism of presenting dual-channel nanoprinting images is delineated in Fig. 2. For each nanobrick, the black dotted line representing a specific intensity has four cross-marked points of intersection, #1, #2, #3, and #4. These intersections indicate that for nanoprinting target 1 to achieve a particular intensity modulation, each nanobrick has four potential orientation angles. For the same nanobrick, the intensity of nanoprinting target 2 can be chosen to be lower or higher than 0.5. Specifically, to realize a higher value modulation, two orientation angles can be chosen, #1 and #2, while to achieve a lower value modulation, two orientation angles can be chosen, #3 and #4. Utilizing this approach, nanoprinting images can be exhibited through both YLP and LCP light, thereby establishing a fresh approach for actualizing dual-channel image displays and enhancing the malleability of the design.

In the far field, owing to the orientation degeneracy's design flexibility mentioned in the near field, each nanobrick can attain the required intensity with two different orientation angles, thereby enabling the accomplishment of a two-step geometric phase encoding. Subsequently, while retaining the nanobrick as a QWP, propagation phase is introduced by sizing the nanobrick's dimension to achieve a five-step propagation phase. Following this, the geometric phase is merged with the propagation phase to generate diverse phase delays for YLP and LCP incident light, leading to the creation of two independent holographic images. Finally, the target phase profile of holography is calculated by the Gerchberg–Saxton (GS) algorithm. In order to apply it to the case of large-angle exit, Rayleigh Sommerfeld diffraction (RS) is employed to calculate the diffraction result. The formula of diffraction can be given by[38]

$$U(x_0, y_0) = \frac{1}{i\lambda}\iint U(x, y)\cos\langle n, r\rangle \frac{\exp(ikr)}{r}\mathrm{d}x\mathrm{d}y, \tag{7}$$

where $U(x_0, y_0)$ and $U(x, y)$ represent the complex-amplitude distribution of electric fields on the holographic plane and metasurface, respectively. λ represents the wavelength of diffraction. $\cos\langle n, r\rangle = z/r$ is the inclination factor. The phase of two holograms can be determined via GS algorithm optimization. From the 10-step phases mentioned above, select the one closest to the two holographic images and subsequently determine the corresponding size and orientation angle.

Figure 3 illustrates the design process for a four-channel metasurface. Initially, Malus's law is employed to calculate the intensity of nanoprinting target 1. This information is then matched with the intensity values in the curve to obtain four candidate orientation angles. Subsequently, the incident light is switched from YLP to LCP light and the intensity of nanoprinting target 2 can be chosen to be lower or higher than 0.5. Out of the four possible orientations, two can qualify and a two-step geometric phase encoding can be achieved. Thereafter, by meticulously designing the dimensions of each nanobrick, a five-step propagation phase can be attained. The geometric phase and propagation phase are then combined to produce different phase delays for YLP and LCP incident light, respectively. Finally, the GS algorithm can be utilized to calculate the target phase. Among the 10-step phases mentioned above, select the one closest to the two holographic images and subsequently determine the corresponding size and orientation angle.

As shown in Fig. 4(a), the proposed metasurface comprises two different components: subwavelength-spaced Si nanobricks

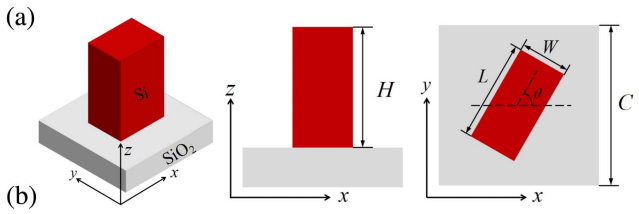

	L (nm)	W (nm)	Cross-transmittance	Propagation phase (rad)
nanobrick1	372	244	0.4575	-2.4217
nanobrick2	396	82	0.4637	-0.8349
nanobrick3	414	126	0.4615	1.0918
nanobrick4	402	184	0.4799	1.9425
nanobrick5	498	192	0.4618	2.7722

Fig. 4. (a) Schematic of a subwavelength-spaced Si nanobrick on a SiO_2 substrate; (b) dimensions of the selected five nanobricks and their cross-transmittance and propagation phase.

and a SiO_2 substrate. Each nanobrick is defined by five structural parameters: cell length C, height H, length L, width W, and orientation angle θ. According to grating formula, to reduce the near-field coupling effect, the cell size should be larger. However, to avoid the high diffraction orders of the metasurface, the cell size should be smaller. In light of this, we opted for a cell length of 700 nm while fixing the nanobrick's height at 1000 nm. To determine the appropriate dimensions, we employed FDTD Solutions (Lumerical Inc., Vancouver, BC, Canada) to perform a scan of the length and width of the Si nanobricks. Specifically, in the simulation, we varied the lengths of the nanobricks from 350 to 520 nm and the widths from 80 to 250 nm with a 2 nm increment at the wavelength of 1310 nm. The details of geometric parameters, cross-transmittances, and propagation phases of the selected nanobricks are listed in Fig. 4(b).

3. Results

3.1. Amplitude control of two polarization states

For the sake of simplicity, and to showcase the amplitude control of two nonorthogonal polarization states, a metasurface sample is designed, labeled M1. The orientation angles of individual nanobricks are determined based on the desired intensity of the nanoprinting images, while the size of each nanobrick remains unaltered. Comprising a total of 100×100 nanobricks, the M1 design spans a dimension of $70\ \mu m \times 70\ \mu m$. The incident light sources are YLP and LCP light, both operating at a wavelength of 1310 nm.

By customizing the orientation angles of individual nanobricks, the intensity of output lights can be regulated by diverse modulation functions. Figure 5(a) illustrates the intensities of different modulation functions in both simulation and theory. Figure 5(b) displays the simulated outcomes.

As the results show, two nanoprinting images can be displayed under both LP and CP light. In contrast to the previous demonstration, the proposed metasurface platform provides a novel method to achieve dual-channel image displays and enhances the malleability of the design.

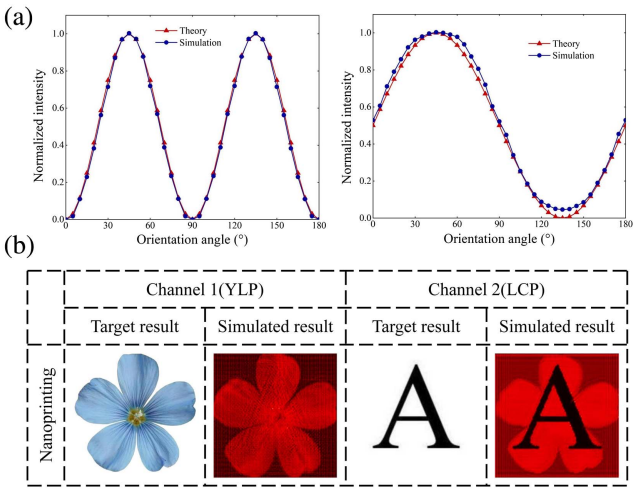

Fig. 5. (a) Simulated and theoretical intensity. (b) Simulation results of the metasurfaces for dual-channel nanoprinting images. The second column shows the nanoprinting images under YLP incident light. The fourth column shows the nanoprinting images under LCP incident light.

3.2. Amplitude and phase control of two polarization states

To showcase the potential for multiplexing the proposed metasurface in two nonorthogonal polarization states, two samples of metasurface have been designed and labeled M2 and M3, respectively. These samples exhibit different nanoprinting and holographic images. The incident light comprises YLP and LCP light, while the wavelength of operation is 1310 nm and the distance between the metasurface and holographic images has been designed to be 30 μm. The inverse operation has been employed to calculate the distribution of nanobricks in terms of their orientation angles and dimensions. Figure 6 depicts the simulated results in both the near field and far field.

As shown in Fig. 6(b), the nanoprinting images in sample 1 are "petal" and "A," and the holographic images in sample 1 are "C" and "B," respectively. The sample 2 shows "flower" and "B" in the near field and "Z" and "D" in the far field. As the results show, these metasurfaces can be multiplexed under two nonorthogonal polarization states to achieve four-channel image displays.

To evaluate the outcomes, we investigate the holographic efficiency of the two holographic images. The holographic image efficiency can be defined as the quotient of the light intensity of the holographic imaging and the input intensity. At the designed wavelength of 1310 nm, the holographic images efficiencies in sample 1 and sample 2 are 20.21% and 19.68%, 18.15% and 19.92%, respectively. In comparison with other metasurfaces, our attained holographic image efficiency is acceptable. Actually, the reduced efficiency of our metasurface results primarily from the nanobricks that serve as a QWP and the polarization conversion rate of the QWP was only 50%.

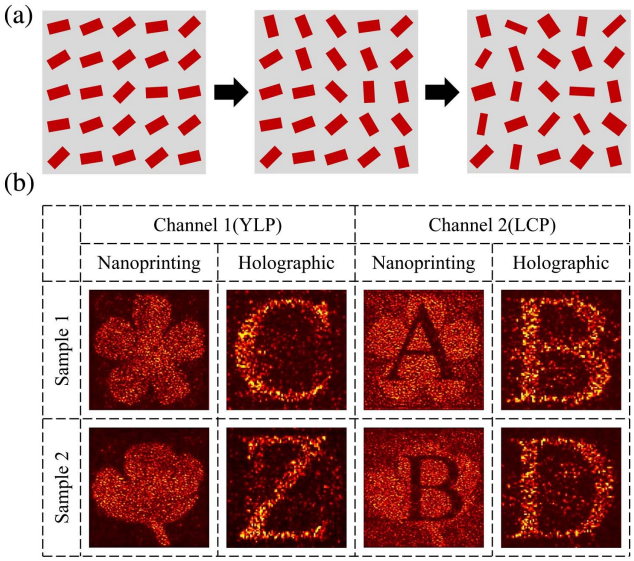

Fig. 6. (a) Design flow of four-channel metasurface; (b) simulation results of the metasurfaces for four-channel image displays. The first column and the second column, respectively, show the nanoprinting images and holographic images in the near field and far field under YLP light. The third column and the fourth column, respectively, show the nanoprinting images and holographic images in the near field and far field under LCP light.

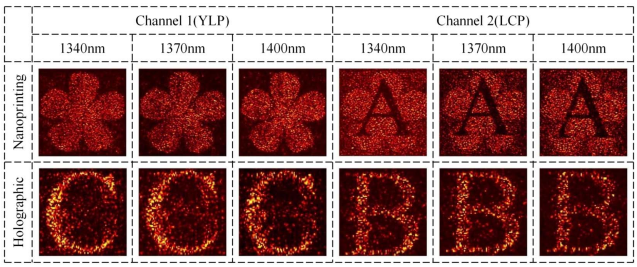

Fig. 7. Simulation results of broadband response. The different columns show the simulation results at different wavelengths (1340, 1370, 1400 nm).

To investigate the broadband property of nanoprinting images in the near field and holographic images in the far field, three YLP lights and LCP lights near the operation wavelengths are utilized to irradiate M2. As demonstrated in Fig. 7, the nanoprinting and holographic images maintain their high quality as the wavelengths span from 1310 to 1400 nm, with intervals of 30 nm. This observation verifies the ability of the metasurface to work in a wide band. Furthermore, when the wavelength deviates more to the designed wavelength, the holographic image will emerge with a larger geometric distortion. This phenomenon can be accounted for as phase mismatch based on diffraction theory.

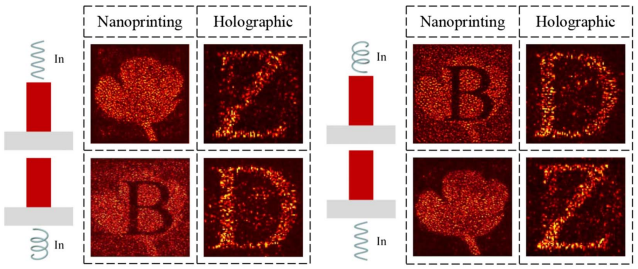

Fig. 8. Simulation results of bidirectional nanoprinting and bidirectional holography. When the direction of incidence polarization states is changed, bidirectional nanoprinting and bidirectional holography can be achieved.

Single-layer metasurfaces that are independent of propagation direction exhibit symmetric optical responses in both forward and backward transmissions. This optical behavior can be observed by altering the direction of propagation. Figure 8 shows that changing the direction of incidence for one of the polarization states can enable bidirectional nanoprinting and bidirectional holography. This metasurface presents a straightforward method to implement these processes in both directions, thereby increasing the practical applications of the technology.

Based on the simulation results, the proposed metasurfaces exhibit the ability to achieve four-channel image displays in two nonorthogonal polarization states within the near-infrared band. As shown in Table 1, our design offers several noteworthy advantages over previous schemes. First, each nanobrick of this single-layer metasurface integrates two sets of amplitude- and phase-modulated channels. Second, the anisotropic nanobricks serve as a QWP, enabling a novel approach to dual-channel image displays and enhancing design flexibility. Finally, bidirectional nanoprinting and bidirectional holography can be achieved by changing the direction of incidence polarization states, offering a simple way to implement bidirectional nanoprinting and bidirectional holography, enhancing their practical applications.

Table 1. Comparison between the Previous Multichannel Supersurfaces and This Article.

	Polarization States	Methods	Unit Cell	Holographic Efficiency
Ref. [31]	Orthogonal polarization states	Interleaved metasurfaces	2 × 2	
Ref. [32]	Orthogonal polarization states	Coherent pixelated metasurfaces	2 × 2	16%
This article	Nonorthogonal polarization states	Modified Malus's law	1 × 1	19%

4. Conclusions

In summary, a single-layer metasurface composed of subwavelength-spaced Si nanobricks on a SiO_2 substrate is designed to achieve four-channel image displays under two nonorthogonal polarization states. In contrast to previous demonstrations, the anisotropic nanobricks act as a QWP. By tailoring the orientation angles of each nanobrick, nanoprinting can be displayed under both LP and CP light. On this basis, the propagation phase is combined with the geometric phase to generate different phase delays, enabling the metasurface to be multiplexed under two nonorthogonal polarization states to achieve four-channel image displays. Each nanobrick of this single-layer metasurface integrates two sets of amplitude- and phase-modulated channels, which can open new possibilities for creating compact multifunctional optical devices, while also enhancing applications in multichannel image displays, information anticounterfeiting, and encryption.

Acknowledgement

This work was supported by the National Natural Science Foundation of China (NSFC) (Nos. 62175070 and 61774062), the Natural Science Foundation of Guangdong Province (No. 2021A1515010352), and the Science and Technology Program of Guangzhou (No. 2019050001).

References

1. H. Ren, X. Fang, J. Jang, J. Bürger, J. Rho, and S. A. Maier, "Complex-amplitude metasurface-based orbital angular momentum holography in momentum space," Nat. Nanotechnol. **15**, 948 (2020).
2. C. Xiong, X. Zhang, Q. Xu, Z. Yao, S. Zhang, T. Wu, X. Chen, Y. Xu, L. Niu, J. Han, and W. Zhang, "Polarization-insensitive amplitude and phase control based on interference metasurface," Appl. Phys. Lett. **121**, 201707 (2022).
3. Z. Deng, M. Jin, X. Ye, S. Wang, T. Shi, J. Deng, N. Mao, Y. Cao, B. Guan, A. Alù, G. Li, and X. Li, "Full-color complex-amplitude vectorial holograms based on multi-freedom metasurfaces," Adv. Funct. Mater. **30**, 1910610 (2020).
4. J. Li, Y. Yuan, Q. Wu, S. N. Burokur, and K. Zhang, "Dual-band independent phase control based on high efficiency metasurface," Chin. Opt. Lett. **19**, 100501 (2021).
5. X. Huang, Z. Liu, Y. Lian, Z. Hu, J. Wu, and J. Wang, "Dynamic beam all-direlectric coding metasurface converter based on phase change materials of GST," Opt. Laser Technol. **159**, 109037 (2023).
6. L. Liu, X. Zhang, M. Kenney, X. Su, N. Xu, C. Ouyang, Y. Shi, J. Han, W. Zhang, and S. Zhang, "Broadband metasurfaces with simultaneous control of phase and amplitude," Adv. Mater. **26**, 5031 (2014).
7. Y. Yuan, S. Sun, Y. Chen, K. Zhang, X. Ding, B. Ratni, Q. Wu, S. N. Burokur, and C. Qiu, "A fully phase-modulated metasurface as an energy-controllable circular polarization router," Adv. Sci. **7**, 2001437 (2020).
8. S. Li, X. Xu, R. M. Veetil, V. Valuckas, R. P. Domínguez, and A. I. Kuznetsov, "Phase-only transmissive spatial light modulator based on tunable dielectric metasurface," Science **364**, 1087 (2019).
9. C. Wang, H. Xu, Y. Wang, C. Zhang, S. Wang, M. Wang, and X. Yang, "Heterogeneous amplitude-phase metasurface for distinct wavefront manipulation," Adv. Photonics Res. **2**, 2100102 (2021).
10. X. Zang, F. Dong, F. Yue, C. Zhang, L. Xu, Z. Song, M. Chen, P. Y. Chen, G. S. Buller, Y. Zhu, S. Zhuang, W. Chu, S. Zhang, and X. Chen, "Polarization encoded color image embedded in a dielectric metasurface," Adv. Mater. **30**, 1707499 (2018).
11. H. L. Zhu, S. W. Cheung, K. L. Chung, and T. I. Yuk, "Linear-to-circular polarization conversion using metasurface," IEEE Trans. Antennas Propag. **61**, 4615 (2013).
12. Y. Chen, X. Yang, and J. Gao, "3D Janus plasmonic helical nanoapertures for polarization-encrypted data storage," Light Sci. Appl. **8**, 45 (2019).
13. G. Zheng, G. Liu, M. G. Kenney, Z. Li, P. He, S. Li, Z. Ren, and Q. Deng, "Ultracompact high-efficiency polarising beam splitter based on silicon nanobrick arrays," Opt. Express **24**, 6749 (2016).
14. Y. Zhang, Y. Cheng, M. Chen, R. Xu, and L. Yuan, "Ultracompact metaimage display and encryption with a silver nanopolarizer based metasurface," Appl. Phys. Lett. **117**, 021105 (2020).
15. Z. Yue, J. Li, C. Zheng, J. Li, M. Chen, X. Hao, H. Xu, Q. Wang, Y. Zhang, and J. Yao, "Manipulation of polarization conversion and multiplexing via all-silicon phase-modulated metasurfaces," Chin. Opt. Lett. **20**, 043601 (2022).
16. Y. Cao, L. Tang, J. Li, C. Lee, and Z. Dong, "Four-channel display and encryption by near-field reflection on nanoprinting metasurface," Nanophotonics **11**, 3365 (2022).
17. X. Zhang, D. Tang, L. Zhou, J. Jiao, D. Feng, G. Liang, and Y. Guo, "Polarization-insensitive colorful meta-holography employing anisotropic nanostructures," Nanoscale **11**, 20238 (2019).
18. X. Ni, A. V. Kildishev, and V. M. Shalaev, "Metasurface holograms for visible light," Nat. Commun. **4**, 2807 (2013).
19. Q. Jiang, G. Jin, and L. Cao, "When metasurface meets hologram: principle and advances," Adv. Opt. Photonics **11**, 518 (2019).
20. Z. Li, Y. Zhang, J. Yuan, Y. Hong, H. Liu, J. Guo, Q. Dai, and Z. Wei, "Three-channel metasurfaces for multi-wavelength holography and nanoprinting," Nanomaterials **13**, 183 (2022).
21. L. Wang, T. Wang, R. Yan, X. Yue, H. Wang, Y. Wang, J. Zhang, and J. Wang, "High performance two-way full colors of transmission and reflection generated by hybrid Mg–TiO_2 metasurfaces," Opt. Laser Technol. **157**, 108770 (2023).
22. H. Zhou, B. Sain, Y. Wang, C. Schlickriede, R. Zhao, X. Zhang, Q. Wei, X. Li, L. Huang, and T. Zentgraf, "Polarization-encrypted orbital angular momentum multiplexed metasurface holography," ACS Nano **14**, 5553 (2020).
23. X. Zhang, X. Li, J. Jin, M. Pu, X. Ma, J. Luo, Y. Guo, C. Wang, and X. Luo, "Polarization-independent broadband meta-holograms via polarization-dependent nanoholes," Nanoscale **10**, 9304 (2018).
24. X. Shang, G. He, L. Li, C. Wang, C. Lu, P. Zhang, J. Niu, and L. Shi, "Controlling brightness in full color nanoprinting by all-dielectric metasurfaces," Appl. Phys. Lett. **122**, 181701 (2023).
25. J. Park, J. H. Kang, S. J. Kim, X. Liu, and M. L. Brongersma, "Dynamic reflection phase and polarization control in metasurfaces," Nano Lett. **17**, 407 (2017).
26. Z. Li, Y. Zhang, H. Huang, S. Qin, K. Jie, H. Liu, J. Guo, H. Meng, F. Wang, X. Yang, and Z. Wei, "Dual-channel metasurfaces for independent and simultaneous display in near-field and far-field," Opt. Express **30**, 18434 (2022).
27. Z. Zhang, Z. Zhang, Z. Tong, M. Yang, J. Guan, Y. Jin, Z. Wei, F. Wang, C. Tan, and H. Meng, "Three-channel metasurface based on simultaneous and independent control of near and far field under a single line light source," Opt. Express **30**, 30936 (2022).
28. J. Deng, L. Deng, Z. Zhou, F. Gao, B. Lv, M. Du, and B. Yan, "Single-sized multifunctional metasurfaces for simultaneous nanoprinting and holography inspired by tri-redundancy," Opt. Express **30**, 29161 (2022).
29. Y. Bao, Y. Yu, H. Xu, C. Guo, J. Li, S. Sun, Z. Zhou, C. Qiu, and X. Wang, "Full-colour nanoprint-hologram synchronous metasurface with arbitrary hue-saturation-brightness control," Light Sci. Appl. **8**, 95 (2019).
30. R. Fu, K. Chen, Z. Li, S. Yu, and G. Zheng, "Metasurface-based nanoprinting: principle, design and advances," Opto-Electron. Sci. **1**, 220011 (2022).
31. Y. Yuan, Q. Wu, S. N. Burokur, and K. Zhang, "Chirality-assisted phase metasurface for circular polarization preservation and independent hologram imaging in microwave region," IEEE Trans. Microw. Theory Tech. **71**, 3259 (2023).
32. Y. Wang, Y. Yuan, Y. Liu, X. Ding, B. Ratni, Q. Wu, S. N. Burokur, G. Hu, and K. Zhang, "Extreme diffraction management in phase-corrected gradient metasurface by fourier harmonic component engineering," Laser Photonics Rev. **17**, 2300152 (2023).

33. M. Liu, W. Zhu, P. Huo, L. Feng, M. Song, C. Zhang, L. Chen, H. J. Lezec, Y. Lu, A. Agrawal, and T. Xu, "Four-channel metasurfaces enabled by simultaneous and independent control of phase and amplitude for orthogonal polarization states," Light Sci. Appl. **10**, 107 (2021).
34. C. Feng, T. He, Y. Shi, Q. Song, J. Zhu, J. Zhang, Z. Wang, D. P. Tsai, and X. Cheng, "Diatomic metasurface for efficient six-channel modulation of Jones matrix," Laser Photonics Rev. **17**, 2200955 (2023).
35. Q. Dai, Z. Guan, S. Chang, L. Deng, J. Tao, Z. Li, Z. Li, S. Yu, G. Zheng, and S. Zhang, "A single-celled tri-functional metasurface enabled with triple manipulations of light," Adv. Funct. Mater. **30**, 2003990 (2020).
36. R. Ren, Z. Li, L. Deng, X. Shan, Q. Dai, Z. Guan, G. Zheng, and S. Yu, "Non-orthogonal polarization multiplexed metasurfaces for tri-channel polychromatic image displays and information encryption," Nanophotonics **10**, 2903 (2021).
37. C. Chen, S. Gao, X. Xiao, X. Ye, S. Wu, W. Song, H. Li, S. Zhu, and T. Li, "Highly efficient metasurface quarter-wave plate with wave front engineering," Adv. Photonics Res. **2**, 2000154 (2021).
38. Q. Wang, E. Plum, Q. Yang, X. Zhang, Q. Xu, Y. Xu, J. Han, and W. Zhang, "Reflective chiral meta-holography: multiplexing holograms for circularly polarized waves," Light Sci. Appl. **7**, 25 (2018).